Project report for SCEC Award 14097: Effect of geothermal operations on earthquake source spectra"

Xiaowei Chen[1] and Jeff McGuire[2]

1. Department of Geology and Geophysics, the University of Oklahoma.
2. Department of Geology and Geophysics, Woods Hole Oceanographic Institution.

Summary:

The borehole network operated by CalEnergy provides high quality dataset for the microearthquakes in the Salton Sea geothermal region. The network was open to public from 2008 to early 2014, which recorded over 7000 earthquakes in the geothermal field; the majority of earthquakes are concentrated in the middle cluster during this time period, and the feature of three sub-clusters remains prominent. With high-resolution earthquake location based on 3D velocity model, we identify clear depth separation between larger ($M \geq 2.5$) and smaller ($M < 2.5$) events in the middle cluster. Our preliminary spectral analysis has revealed reduced fault strength near the main fault that hosted the M5 2005 earthquake swarm (low stress drop), where two main earthquake bursts in late 2009 and 2010 occurred. In the middle cluster, stress drop increases from 1.5 MPa closest to injection wells to 5 MPa at 300 m from injection wells. Beyond 0.3 km, the stress drop is nearly constant, suggesting that the spatial window of directly induced seismicity maybe limited in 300m from injection wells. The results suggest complex interaction between fluid and faults in the geothermal field. We are continuing to integrate the stress drop, the velocity model, and the high-resolution location to get better understanding of the geomechanical process of the seismicity in the geothermal field.

Intellectual merit:

The research contributes to integrated understanding of the geomechanical process within the active geothermal field. The new findings of reduced stress drop near the main fault zone, and stress drop distance dependence within 300m is important for understanding the spatial influence window of injection activity, and interaction between fluid circulation and pre-existing weak zones.

Broader impacts:

The project results are beneficial for learning earthquake hazards, risks and earthquake physics. Due to the recent increase in earthquakes in central US, the students at the University of Oklahoma are interested in learning more about induced seismicity, and enrolled in my seminar on "induced seismicity". A master student at OU is currently working on this project with Xiaowei Chen. The research results are relevant to a few ongoing research projects at other institutions, for

example, the shear-wave velocity changes in the geothermal field by Jeff McGuire at WHOI, the earthquake detection by Zhigang Peng at Gatech.

Technical report:

1. Project objective:

We plan to use the Borehole network deployed by CalEnergy with open access data from 2008 to 2014, to investigate detailed spatial and temporal variations of earthquake stress drop within the three small clusters defined by geothermal injection/production well locations. With these results, we would like to address:

(1) Are there temporal changes in earthquake source spectra in response to different stages of geothermal operation? Are these variations link to fluid pressure variations due to changes in operation?
(2) What is the spatial influence window of the geothermal injection activities? Is there potential to trigger larger events in this area?
(3) Are there differences in earthquake responses among the three clusters in response to different injection parameters?

2. Research progress

Data

We download and archive event-based waveform from southern California earthquake data center from 2008 to 2014. During this period, Calenergy shared the borehole network to the general public for academic research. The borehole network is consisted of 8 stations, providing ideal azimuthal coverage of the microearthquakes in the geothermal field. The magnitude of completeness is about 1.0 throughout the study period. A 3D P-wave velocity model available for relocation and velocity correction was derived in McGuire et al., 2015, with combined active source and earthquake phase arrivals. The 3D velocity model found up to 50% lateral variations of P-wave velocity.

Earthquake location

As the first step, we perform tomoDD relocation for 7348 earthquakes using the 3D velocity model and catalog phase picks, and calculate differential times for event pairs using catalog phase picks. We use three iteration settings (see below):

```
* NITER WTCCP WTCCS WRCC WDCC  WTCTP  WTCTS   WRCT WDCT WTCD DAMP
JOINT THRES
   5  0.01  0.01  10  10  1.0 0.75    6   4  100  400 0  .5
   5  0.01  0.01  10  10  1.0 0.75    4   3  100  400 0  .5
   5  0.01  0.01   6   4  1.0 0.75   0.6  3  10   200 0  .5
```

The iteration is designed to allow higher residual at the first step, and progressively reduce the residual threshold. The goal for this step is to get better constraint of the absolute locations of the earthquakes, in order to investigate their relationship to injection and production wells.

The improvement of the location is significant, the average distance shift reduced from (995 m, 1063 m, 846 m) at the first iteration to (18m, 21m and 36m) during the final iteration. The average origin time reduced from > 1000 ms to 4 ms during the final iteration. The earthquake locations are considerably tighter than the original catalog locations. The majority of the microearthquakes are concentrated within the middle cluster.

There is also clear spatial separation among larger ($M \geq 2.5$) and smaller ($M<2.5$) events in the middle cluster: the larger events are located within the upper 3 km, and an ellipsoid of microseismicity is located beneath the larger events. A few larger events are located deeper than 4 km. For depth between 3 km to 4 km in the middle cluster, there is an absence of larger events. In this step, we used 522587 catalog P differential times, 54829 catalog S differential times, 65088 absolute catalog P arrival times, and 14334 absolute catalog S arrival times.

Next, we compute waveform cross-correlation for each earthquake with the nearest 500 earthquakes. The nearest 500 events are selected based on the tomoDD relocations. We only use P-wave cross-correlation on the vertical channels, and S-wave cross-correlation on horizontal channels. The cross-correlation window is -0.3s before and 0.8s after P-wave picks (or predicted arrival time based on averaged 1D velocity model), -0. 5 s before and 1.0 s after S-wave picks (or predicted arrival time based on averaged 1D velocity model assuming Vp/Vs ratio of 1.732). The time window is designed to avoid S-wave in the P-wave window. The minimum cross-correlation value to use a differential time is 0.65, and only pairs with at least 8 good correlation (including both P and S), and average cross-correlation > 0.65 are included. We use the method "growclust" described in Matoza et al., 2013 to relocate these events (for details, please refer to Matoza et al, 2013). The result additionally reveals detailed seismicity streaks. And two subparallel faults to the eastern side of the geothermal field.

The absence of larger events in the middle cluster between 3 and 4 km possibly suggest concentration of immediately induced seismicity due to geothermal production. While the larger events are located along the faults that hosted the M5 events in 2005, suggesting that these events primarily occur along pre-existing weak zones. In the following spectral analysis, our locations are based on the locations derived via cluster analysis and waveform cross-correlation.

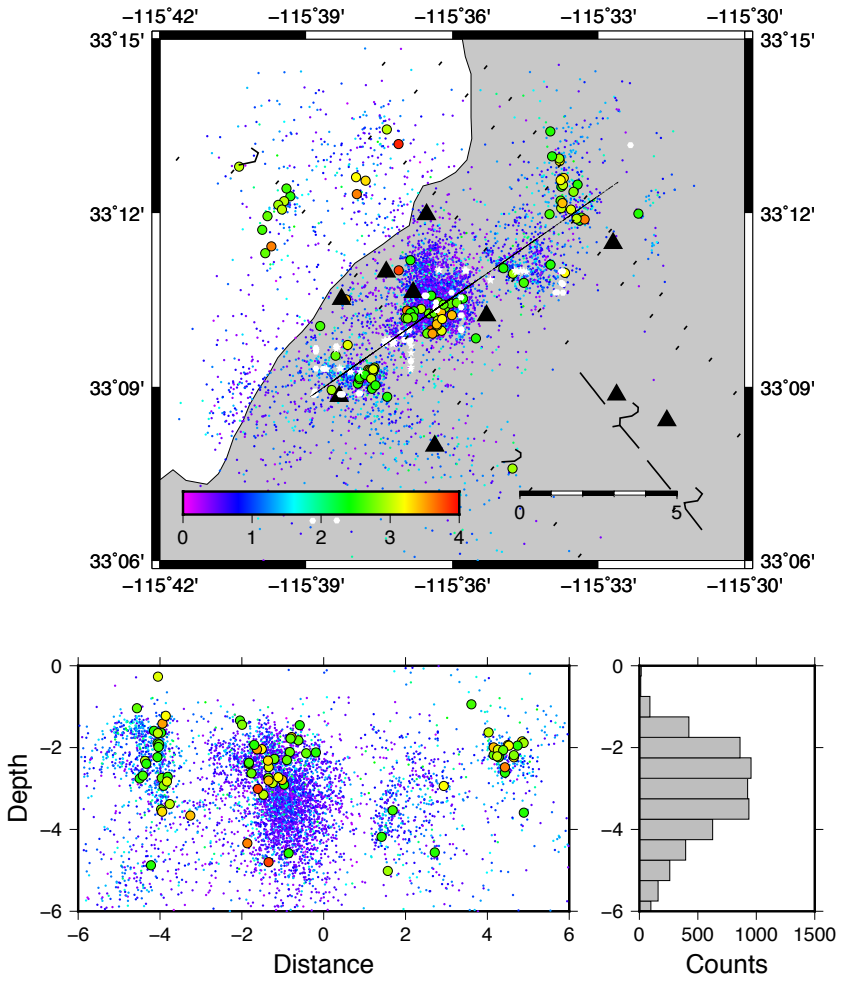

Figure 1. TomoDD relocation based on catalog phase picks. Top: Map view of all earthquakes, events are colored by their magnitude, according to the colorbar in the map. Events outlined by black lines are events with M ≥ 2.5. White dots are geothermal injection wells, and white stars are geothermal production wells. Bottom left: Cross-section view of earthquakes along the profile with black line in the top figure from west to east. Bottom right: Histogram of depth distribution of all events. The absence of larger events in the middle cluster from 3 to 4 km is visually clear.

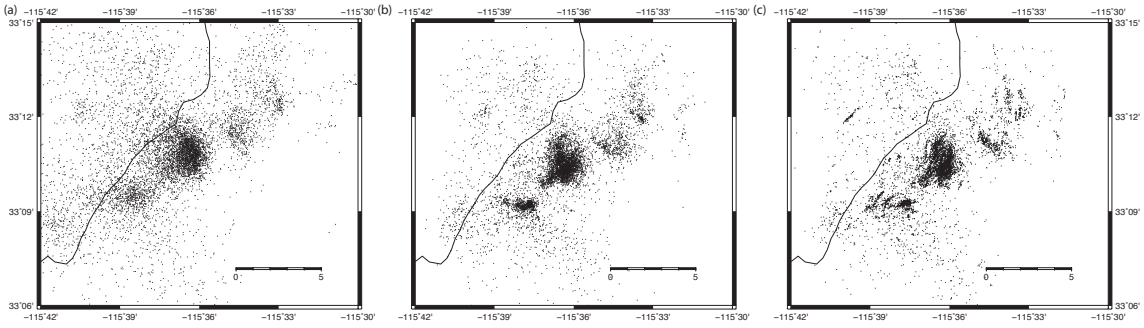

Figure 2. Comparison of the three locations. (a) Original catalog locations. (b) tomoDD relocations. (c) Cluster relocation based on cross-correlation.

P-wave spectral analysis

In Chen and Shearer 2011, we used all available stations in southern California, and computed P-wave spectra using 1.28s time window immediately after catalog P-wave picks or predicted arrival times based on averaged 1D velocity model for southern California. Here, we focus on the waveform recorded by the borehole network, and use a 0.5 s time window – in order to avoid contamination of S-wave arrivals for close-by stations (S-P time is less than 1s in some cases at station ELM). We use the multitaper method (Prieto et al, 2009) to compute P-wave spectra. We only use spectrum that have minimum signal-to-noise ratio of 3 between 5 to 15 Hz, and 2 between 15 to 20 Hz.

The EN network has a uniform 100 Hz sampling rate, therefore, the maximum frequency to resolve is 50 Hz. We sub-sample the spectra at equal log-frequency interval, in order to downweight the contribution from high-frequency points. We applied the stacking method from Shearer et al., 2006 paper to deconvolve path terms, stations terms, and event terms sequentially. In recognition of the relative spatial/depth separation between small and larger events in the middle cluster, we first focus on the middle cluster, where the majority of seismicity are located during the study period.

We use event spectra averaged from at least 5 stations, and compute averaged spectra for each 0.2 magnitude bin. We solve for an empirical green's function with Brune source model. The following figure is the stacked spectra for each magnitude bin. After shifting spectra along the assumed self-similarity line, the spectra are approximately aligned along the same line, suggesting self-similarity for earthquakes in the middle cluster.

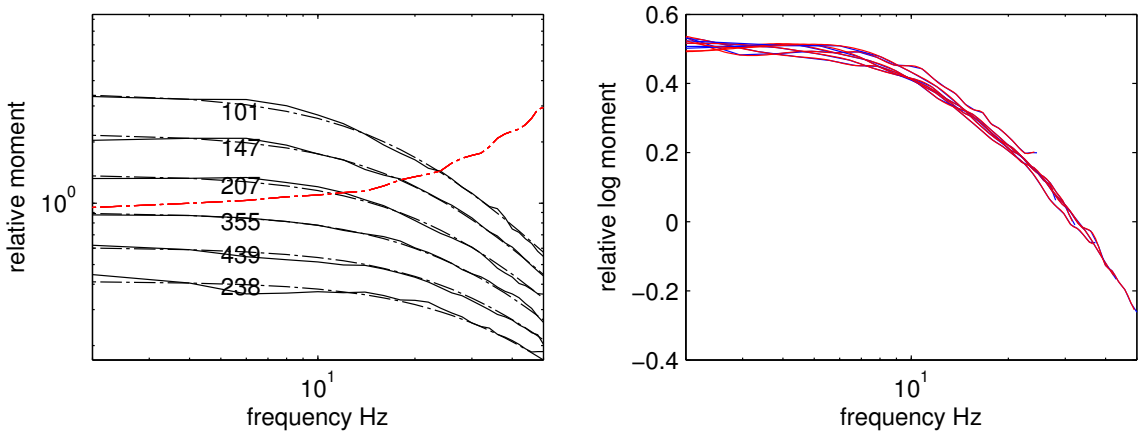

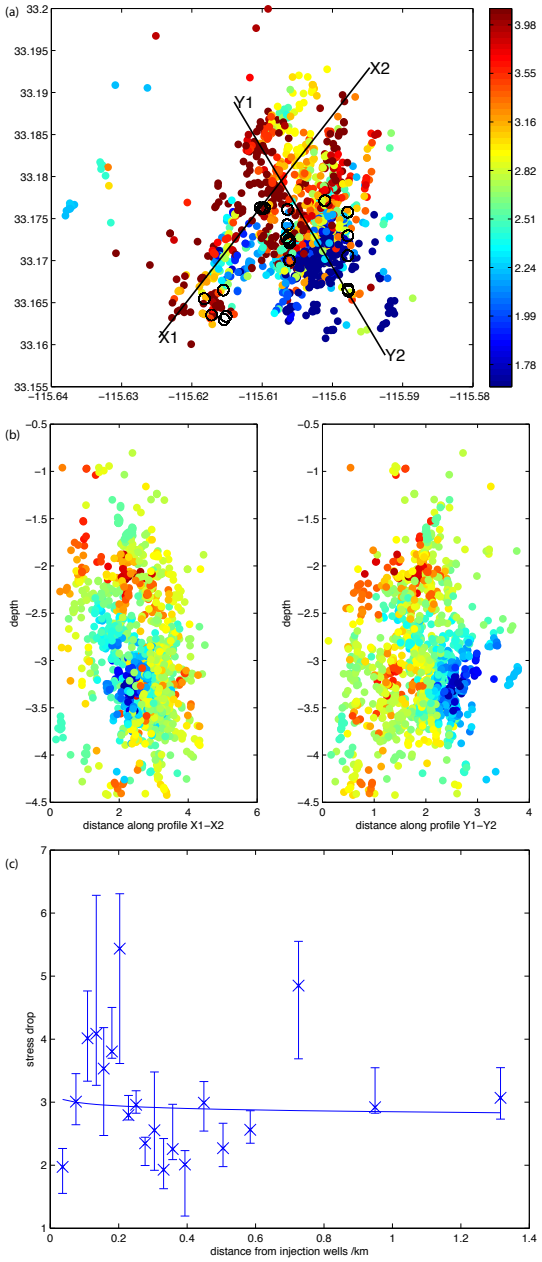

Figure 3. Left: averaged spectra for each magnitude bin from 0.5 to 2.3. Numbers indicate the number of individual event spectra included to estimate average. Right: spectra shifted along moment^(-1./3.) line, as predicted from self-similarity.

We then solve for event-specific EGF with 200 nearest neighbors, and obtained stress drop estimates for 1362 events with the assumed Brune's source model. The results are intriguing – we found low stress drop near the main fault zone, where the majority of larger events are produced, and injection-well-distance dependent stress drop increase up to 300 m, a distance consistent with previous studies of fracturing induced seismicity in enhanced geothermal field site (e.g., Allmann et al, 2010).

Figure 4. (a) Map view of stress drop in the middle cluster after applying spatial-median filter (average stress drop from nearest 50 events). Black circles are injection wells. X1-X2 and Y1-Y2 mark two profiles. (b) Left: Cross-section view along profile X1-X2; Right: Cross-section view along profile Y1-Y2. (c) Stress drop versus distance (from nearest active injection wells). The low stress drop near the main fault zone (southeastern portion) is clear. The vertical errorbars are 25% and 75% of stress drop in each distance bin.

In Progress:

We are continuing to investigate details for the other clusters, in particular, the eastern-ward expansion of the seismicity is consisted of two sub-parallel faults ruptured in 2013 and 2014, respectively, primarily include M ≥ 2.5 earthquakes. What is the relationship between this cluster and the easternmost injection well? What is the stress drop of these events? We are also working on characterizing the uncertainties in stress drop measurement in order to confirm the reliability of the above spatial variations.

We are also in the process of including S-wave in the analysis. We have added manual picks (from Meng and Peng, 2014) and additional automatic S-picks to the database. S-wave contributed to over 80% of radiated energy, and source parameters from S-wave may help to better understand the earthquake hazard and ground motion expected from these earthquakes.

The goal is to integrate various dataset to gain a comprehensive understanding of the mechanical process of induced seismicity in the geothermal field.

Reference:

Allmann, B. P., A. Goertz and S. Wiemer (2011) Stress drop variations of induced earthquakes at the Basel geothermal sites, Geophysical Research Letters, VOL. 38, L09308, doi:10.1029/2011GL047498.

Chen, X., and P. M. Shearer (2011), Comprehensive analysis of earthquake source spectra and swarms in the Salton Trough, California, *J. Geophys. Res.*, *116*(B09309), doi:10.1029/2011JB008263.

Matoza, R. S., P. M. Shearer,G. Lin, C. J.Wolfe, and P. G. Okubo (2013), Systematic relocation of seismicity on Hawaii Island from 1992 to 2009 using waveform cross correlation and cluster analysis, J. Geophys. Res. Solid Earth, 118, 2275–2288, doi:10.1002/jgrb.50189.

Meng, X. and Z. Peng (2014), Seismicity rate changes in the San Jacinto Fault Zone and the Salton Sea Geothermal Field following the 2010 Mw7.2 El Mayor-Cucapah Earthquake, *Geophys. J. Int.*, doi: 10.1093/gji/ggu085.

Prieto, G. A., R. L. Parker and F. L. Vernon III (2009), A fortran 90 library for multitaper spectrum analysis. Computers & Geosciences.